MICROTUBULAR ORIGIN OF MITOTIC SPINDLE FORM BIREFRINGENCE

Demonstration of the Applicability of Wiener's Equation

HIDEMI SATO, GORDON W. ELLIS, and SHINYA INOUÉ

From the Program in Biophysical Cytology, Department of Biology, University of Pennsylvania, Philadelphia, Pennsylvania 19174

ABSTRACT

Meiosis I metaphase spindles were isolated from oocytes of the sea-star *Pisaster ochraceus* by a method that produced no detectable net loss in spindle birefringence. Some of the spindles were fixed immediately and embedded and sectioned for electron microscopy. Others were laminated between gelatine pellicles in a perfusion chamber, then fixed and sequentially and reversibly imbibed with a series of media of increasing refractive indices.

Electron microscopy showed little else besides microtubules in the isolates, and no other component present could account for the observed form birefringence. An Ambronn plot of the birefringent retardation measured during imbibition was a good least squares fit to a computer generated theoretical curve based on the Bragg-Pippard rederivation of the Wiener curve for form birefringence. The data were best fit by the curve for rodlet index (n_1) = 1.512, rodlet volume fraction (f) = 0.0206, and coefficient of intrinsic birefringence = 4.7×10^{-5}. The value obtained for n_1 is unequivocal and is virtually as good as the refractometer determinations of imbibing medium index on which it is based. The optically interactive volume of the microtubule subunit, calculated from our electron microscope determination of spindle microtubule distribution ($106/\mu m^2$), 13 protofilaments per microtubule, an 8 nm repeat distance and our best value for f, is compatible with known subunit dimensions as determined by other means.

We also report curves fitted to the results of Ambronn imbibition of Bouin's-fixed *Lytechinus* spindles and to the Noll and Weber muscle imbibition data.

Fine structure and molecular orientation in cell organelles can be analyzed by polarized light microscopy. By nondestructive means, and in a continuous temporal framework, one can use birefringence (BR) analysis to pinpoint the occurrence and alteration of anisotropic molecular organization in volumes under 10^{-9} μl.

The physiology of spindle fibers has been extensively studied in living cells through measurement of BR changes (Inoué and Sato, 1967; Sato, 1975; Inoué and Ritter, 1975). Reversibly depolymerizable labile fibrils were shown to make up the birefringent fibers, and the nature of the molecular equilibrium was determined.

The positive BR of spindle fibers parallels the distribution and behavior of microtubules seen

with the electron microscope. Rise and fall of fiber BR is accompanied by increase and decrease of tubule concentration. We therefore postulated that microtubules are responsible for spindle fiber BR (Inoué and Sato, 1967). In isolated spindles, BR shows exclusive proportionality to the quantity of tubulin, the subunit protein of microtubules (Stephens, 1972).

Recently pure tubulin has been isolated and polymerized to form labile microtubules in vitro (Weisenberg, 1972; Olmsted and Borisy, 1973). As reviewed elsewhere (Inoué and Ritter, 1975; Inoué et al., 1975), the associative properties of this protein follow closely the polymerization-deploymerization properties of microtubules deduced from spindle fiber BR in living cells.

We now report our analysis of the microtubular origin of spindle fiber BR by demonstrating: first, the fit of the Wiener form BR curve to the measured BR of isolated carefully imbibed spindles; and secondly, the concordance of the rodlet volume fraction defining the best fit Wiener curve with the volume fraction of microtubules calculated from electron microscopy, X-ray diffraction, and hydrodynamic data.

The BR of mixed bodies composed of oriented rodlets or platelets whose thicknesses are well below the wavelength of light is believed to arise from two sources: (a) an intrinsic BR due to the intramolecular anisotropy of the rodlets or platelets; and (b) a textural or form BR due to the anisotropic arrangement, or texture, of the fine structure. Wiener (1912) and Bragg and Pippard (1953) have derived equations which relate the form BR in terms of dielectric anisotropy to: the volume fraction occupied by the rodlets or platelets; their refractive index (n_1) or dielectric constant ($\epsilon_\nu = n_\nu^2$, for nonabsorbing material measured at frequency ν, see e.g. Born and Wolf, 1959, p. 91); and the refractive index (n_2) of the second phase in which the rodlets or platelets are immersed.

Experimentally, Ambronn and Frey (1926) have devised an imbibition method which allows one to determine the form and intrinsic BR contributions in mixed bodies. The intrinsic BR is taken as constant while the form BR varies, as described by the Wiener formula, with the refractive index of the imbibing medium (n_2). The measured BR is the sum of the two and therefore equals the intrinsic BR when the form contribution becomes zero, namely when $n_1 = n_2$.

MATERIAL AND METHODS

Choice of Experimental Material

For analyzing the form BR contributed to spindles by microtubules, we have chosen to use isolated meiotic spindles from oocytes of the sea-star *Pisaster ochraceus*. The choice of isolated spindles rather than of spindles in fixed whole cells was predicated upon the following considerations. (a) Thorough imbibition of intertubular space with media of defined refractive index is essential for exact form BR analysis. (*b*) The dimensions of the specimen must be readily measurable. The dimensions moreover must not change by fixation, imbibition and dehydration. (*c*) Light scattering and BR from extraneous sources must be held to a minimum. Isolated spindles can be sufficiently clean that optical and chemical influences of surrounding cytoplasm are minimum.

The meiosis I spindle can be isolated in large quantity from *P. ochraceus* oocytes. These isolates are reliably clean (Fig. 1), and, in the regions between the metaphase chromosomes and the poles, show little else than microtubules (Figs. 2 and 3). Unlike the spindle in mitotic division, whose dimensions, overall BR, and BR distribution vary rapidly with time and progression of mitosis, the *Pisaster* meiosis I spindle is arrested in metaphase and yields isolates of uniform BR and dimensions. Moreover, the BR of the isolates, which remained close to the value in life, was unchanged upon fixation; and the isolates could be imbibed in a way that the same BR returned when the imbibing medium index was brought back to the original value.

Isolation of Pisaster Spindle

Mature oocytes were obtained by treating isolated sea-star ovaries with 10^{-6} M 1-methyl adenine (Kanatani et al., 1969) in artificial sea water (Cavanaugh, 1964). 1 mg/ml Pronase (ICN K & K Laboratories, Inc., Plainview, N. Y.) and 0.1% mercaptoethylgluconamide (MEGA; Cyclo Chemical, Division of Travenol Laboratories Inc., Los Angeles, Calif.) have been used to activate and remove the fertilization membrane. Spindles are isolated in quantity from these demembranated oocytes at 13°C in 12% hexylene glycol, pH 6.3 following the method described by Bryan and Sato, 1970. The isolation medium is essentially the same as that described for sea urchins by Kane (1962 and 1965). Isolated spindles are stored in isolation medium at 4°C. All imbibition experiments were carried out on spindles not more than 3 h (typically within 40 min) from isolation.

Imbibition Procedure

We took freshly isolated *Pisaster* spindles, transferred them in the isolation medium (12% hexylene glycol) onto a stress-free microscope cover slip flamed and coated with a thin pellicle of gelatin, covered the spindles with another pellicle of gelatin, and assembled the whole

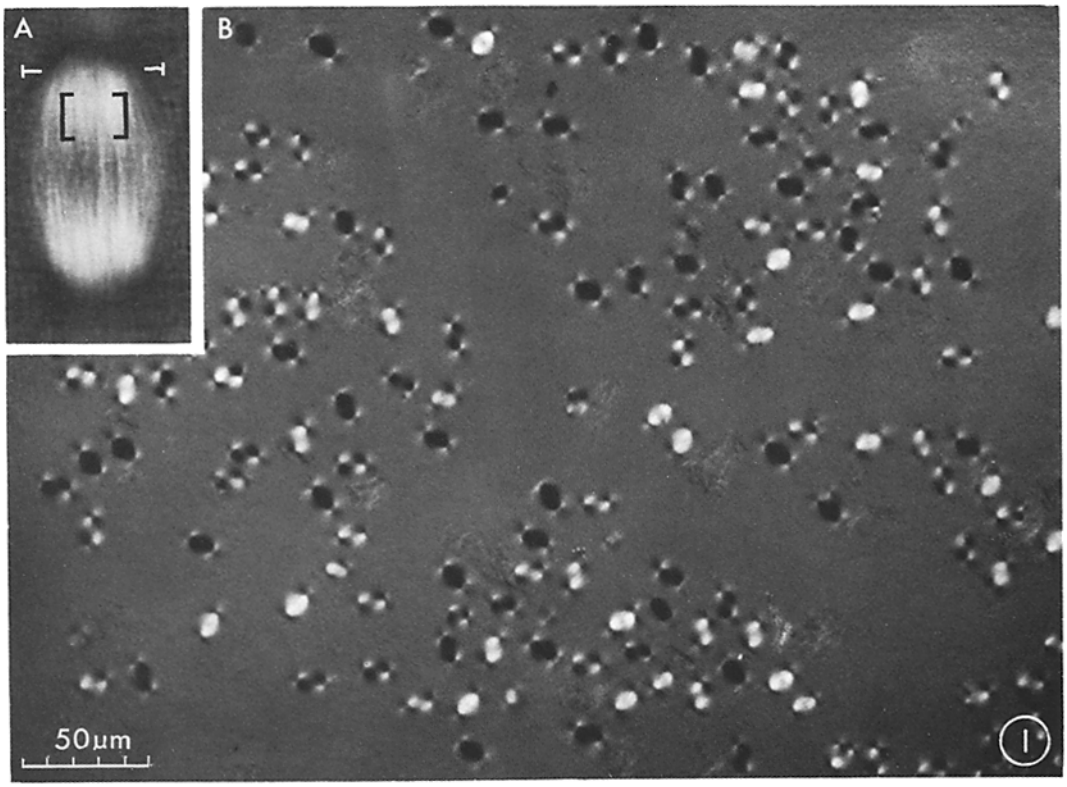

FIGURE 1 Meiosis I spindles from mature oocytes of *P. ochraceus* isolated in hexylene glycol after pronase-MEGA treatment. (A) Spindle birefringence is determined by measuring the retardation (see Fig. 4) in the area surrounded by black brackets. White bars specify the position corresponding to the electron micrograph in Fig. 3. × 2,250 (B) Clean mass isolation of *Pisaster* spindles is shown at lower magnification. Polarization microscopy, × 330.

sandwich as the upper element in a modified "Rose" type perfusion chamber. The fixative and imbibition media were perfused through this chamber with constant velocity so that they penetrated the spindles by diffusion through the gelatin sandwich which also held the spindles securely in place. The gelatin pellicles were prepared at the time of use by dipping a 3 cm diameter platinum loop into a warm (32–38°C) solution of 1%–2% gelatin-isosmolar salt solution (19:1 mixture of 0.56 M NaCl and 0.56 M KCl). Application of this method of cell support and perfusion (developed by Molè-Bajer and Bajer, 1968) was essential for successful perfusion without distortion or loss of the spindles.

After fixation in 3% glutaraldehyde-12% hexylene glycol (pH 6.3 with 10 mM phosphate buffer), the spindle was imbibed with the sequence of solutions listed in Table I. Each successive medium was serially diluted and exchanged gradually to avoid spindle collapse or irreversible BR change. Also, slow exchange is needed to dissipate the heat evolved with each successive mixing of dimethyl sulfoxide (DMSO) with aqueous solution. The transition from DMSO to benzene and the reverse are especially critical points since at these transitions the spindle structure and BR may change irreversibly. This transition into the nonpolar medium appears to be critical for successful imbibition of many cellular structures. The use of benzyl alcohol between DMSO and benzene helps to alleviate this difficulty.

Even with these precautions, some reagents appear to introduce inherently irreversible changes. For this reason, we have avoided the use of glycerol above 30% concentration or high concentrations of hexylene glycol.

We stress the need to qualify all data by the success of reversibility. From the many measurements we have made, we have used data points only from those specimens which showed successful and complete reversal of BR and which showed no change in their microscopic dimensions. Once the data were collected according to these criteria, no data were discarded for the form BR analysis.

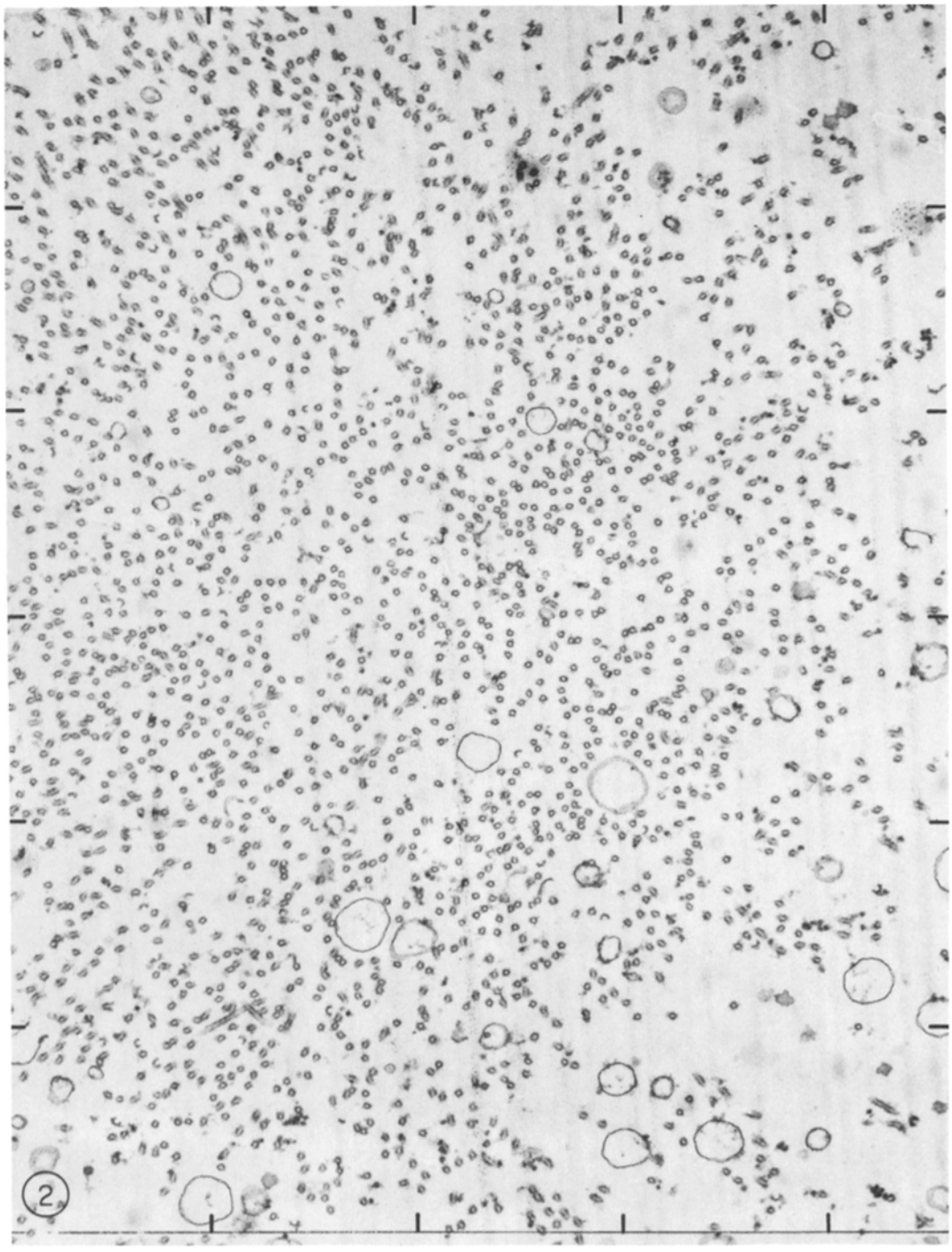

FIGURE 2 Thin cross-section electron micrograph of isolated spindle of *P. ochraceus*. The spindle was sectioned in the mid-region indicated by the bracket in Fig. 1 A. The microtubules in the mid-spindle region are mostly aligned parallel to the spindle axis. This is one of the micrographs used for counting the number of microtubular cross sections per unit area. Grid coordinates 1 μm interval. × 30,500.

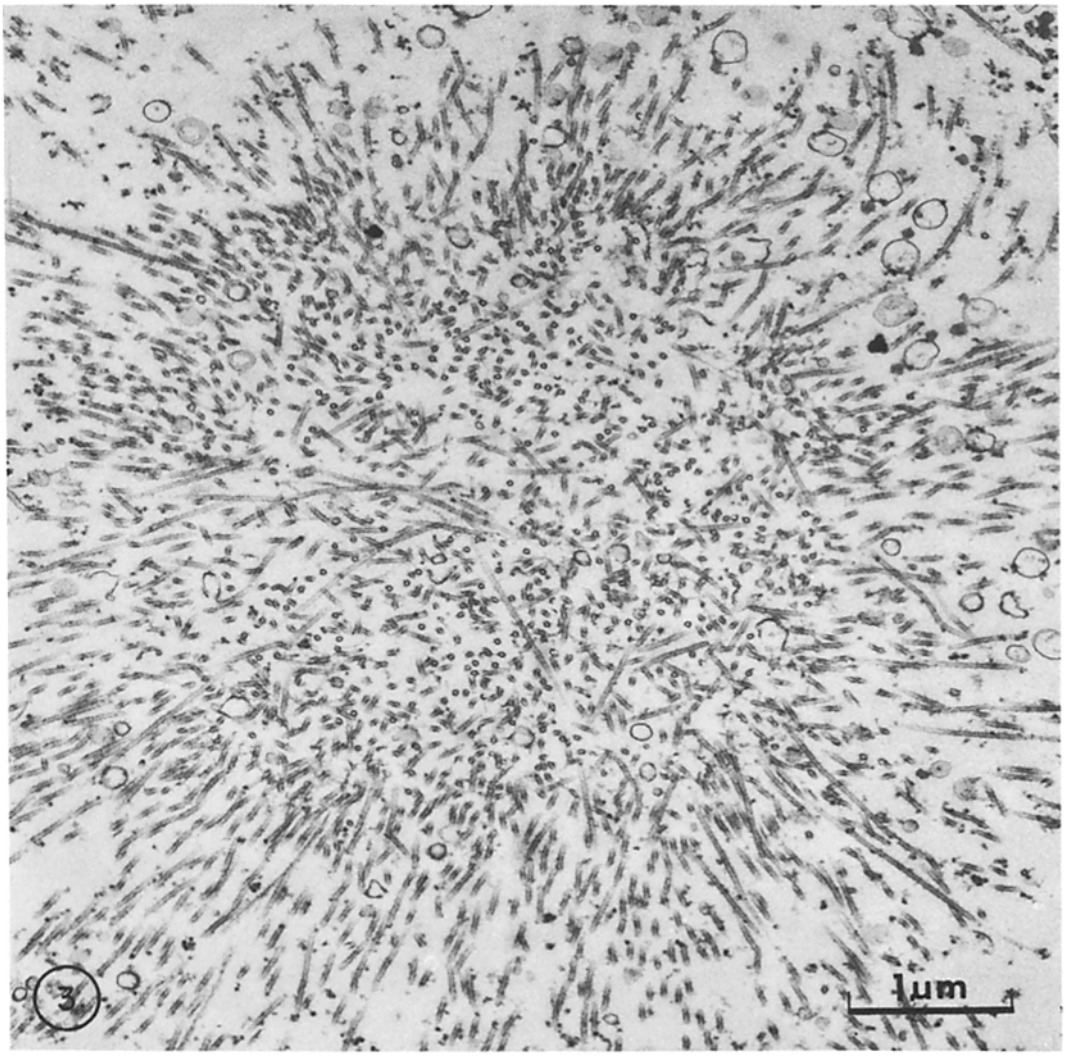

FIGURE 3 Cross section of the polar region (Fig. 1 A white bars) of an isolated metaphase spindle of *P. ochraceus* is mainly occupied by microtubules and little else. Some of the vesicles in the photograph are degenerated mitochondria resulting from the isolation and fixation procedures. × 22,000.

Retardation Measurements

A Leitz Ortholux-Pol (E. Leitz, Inc., Rockleigh, N. J.) microscope was equipped with rectified (Inoué and Hyde, 1957) strain-free optics (American Optical Corp., Scientific Instrument Div., Buffalo, N. Y. and Nippon Kogaku K. K., Toyko, Japan), and with a Polaroid HN-22 nonlaminated sheet polarizer (Polaroid Corp., Cambridge, Mass.) mounted beneath the condenser. All measurements were made with the 40× numerical aperture (NA) 0.65 objective. With the built-in Leitz analyzer, the extinction factor ($I_{parallel}/I_{crossed}$) of the system reached 5×10^4. The output of an Osram HBO-200W L-2 mercury are lamp (Osram GmbH, Berlin-München, West Germany) was filtered with at least one Corning no. 4602 (Corning Glass Works, Optical and Filter Division, Corning, N. Y.) heat-absorbing filter followed by a high transmission type B-2 Baird Atomic Interference filter (Baird Atomic, Inc., System Components Division, Bedford, Mass.) to provide intense illumination by mercury green light at 546 nm. A Zeiss Brace-Köhler compensator (Carl Zeiss, Inc., New York, N. Y.) with a retardance of $\lambda/25$ was used to measure spindle retardation. The isolated spindle

TABLE I

Sequence of Imbibition Media

	Refractive index of imbibition medium (n_z)
1. 12% Hexylene glycol, pH 6.3*	1.348
2. 12% Hexylene glycol-3% glutaraldehyde, pH 6.3*	1.348
3. 12% Hexylene glycol, pH 6.3*	
4. 2% DMSO-12% hexylene glycol	
5. 4% DMSO-12% hexylene glycol	
6. 8% DMSO-12% hexylene glycol	
7. 14% DMSO-12% hexylene glycol	1.367
8. 20% DMSO-12% hexylene glycol	
9. 30% DMSO-12% hexylene glycol	1.390
10. 40% DMSO-12% hexylene glycol	1.404
11. 50% DMSO-12% hexylene glycol	
12. 60% DMSO-12% hexylene glycol	
13. 70% DMSO-12% hexylene glycol	
14. 80% DMSO-12% hexylene glycol	1.455
15. 90% DMSO-12% hexylene glycol	
16. DMSO	1.473
17. DMSO-benzyl alcohol (50:50)	
18. Benzyl alcohol	
19. Benzyl alcohol-benzene (50:50)	
20. Benzene	1.501
21. Benzene-nitrobenzene (75:25)	
22. Benzene-nitrobenzene (50:50)	
23. Benzene-nitrobenzene (25:75)	
24. Nitrobenzene	1.556
25. Nitrobenzene-iodobenzene (75:25)	
26. Nitrobenzene-iodobenzene (50:50)	
27. Nitrobenzene-iodobenzene (25:75)	
28. Iodobenzene	1.622
29–55 Reversal of above sequence to step 3	
56. Artificial sea water (MBL-formula)	1.339

The refractive indices of solutions were determined by a Leitz-Jelly Micro-Refractometer (Leitz Wetzlar, West Germany) using 546 nm light at 20°C. Hexylene glycol lot number 916146, obtained from Union Carbide, Morristown, N. J. Dimethyl sulfoxide (DMSO) obtained from Crown Zellerbach Corp., Camas, Wash. Benzyl alcohol, benzene, nitrobenzene and iodobenzene obtained from Eastman Organic Chemicals Div., Eastman Kodak Co., Rochester, N. Y.

* pH adjusted with ca. 10 mM phosphate buffer.

was oriented at 45° to the polarizer axis, and the region indicated in Fig. 1 A was compensated (Fig. 4) to measure the retardation arising from the BR of parallel microtubules in that region.

Spindle retardation was determined according to the formula:

$$\sin 2\theta \cdot \sin (\Delta/2) = - \sin 2\theta_c \cdot \sin (\Delta_c/2) \qquad (1)$$

where θ is the azimuth orientation of the specimen (here maintained at 45° ± 5°); θ_c is the azimuth angle at which the Brace-Köhler compensator compensates (Fig. 4) the specimen; Δ is the specimen retardation and Δ_c the retardance of the compensator, both expressed in degrees (e.g. see Hartshorne and Stuart, 1960).

Effect of Numerical Aperture on Retardation Measurement

Some experimenters have expressed concern regarding the accuracy of birefringent retardation measurements made at the high objective and condenser apertures required for good resolution. The common thought is that the oblique rays traveling through the specimen follow a longer path through the birefringent material and therefore may suffer a greater retardation than for rays nearer the microscope axis. In the present case the shape of the spindle is such that all rays traveling nearly perpendicular to the spindle axis will have a similar optical path, while the oblique rays traveling in a plane parallel to the spindle axis have a somewhat longer distance to travel, but will experience a decreasing BR. This and the convergent geometry of the microtubules at the spindle ends precludes an easy prediction of the optical path for such rays. Consequently we have measured the birefringent retardation of a number of freshly isolated spindles from *Lytechinus pictus* eggs at three different values of objective and condenser numerical aperture (Nikon rectified optics: 10×, 0.25 NA, objective and condenser matched; 20×, 0.4 NA, objective and condenser matched; and 40×, 0.65 NA, condenser NA = 0.52). For 45 spindles, we obtained the following numerical averages of the retardation: 10×, 3.242 ± 0.095 nm; 20×, 3.207 ± 0.113 nm; 40×, 3.193 ± 0.103 nm. Therefore, we conclude that for measurement of spindles with rectified-optics, no difference in retardation will be found with any of the dry objectives.

Electron Microscopy

Metaphase spindles isolated at 13°C, the optimum physiological temperature for this specimen (Sato and Bryan, 1968), were immediately cooled to 4°C after isolation and washed twice in cold isolation medium by centrifugation at 1,250 *g* for 5 min.

All of the following steps for fixation and dehydration were carried out at 4°C. The use of hexylene glycol in the fixative and dehydration solutions prevents the alteration of spindle BR during these steps (Inoué and Sato, 1967).

Small pellets of isolated spindles were fixed for 30 min in 3% glutaraldehyde-12% hexylene glycol solution at

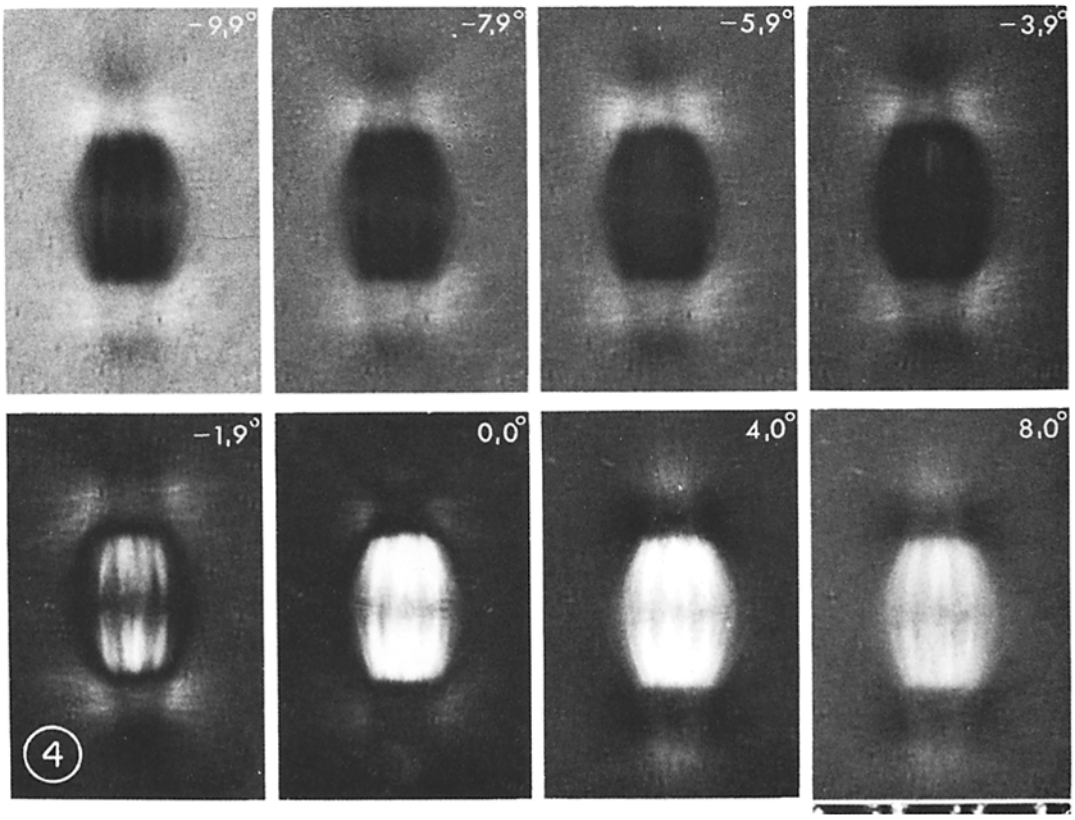

FIGURE 4 Appearance of a single spindle at various compensation angles (white letters on the right shoulder of each photograph). Between crossed polarizers, the spindle is oriented with its slow axis at +45°. As the λ/25 Brace-Köhler compensator is turned, the areas with lower retardation are first compensated (−1.9°) leaving the more highly retarding spindle fibers shining above the dark, compensated areas. With further rotation of the compensator (−3.9°, −5.9°) the chromosomal fibers are still not yet compensated. At −7.9° they are exactly compensated, while at −9.9° the more highly retarding fibers are clearly darker than their surrounding. At 0.0° the background is at extinction position. First mitotic spindle of the fertilized egg of *L. pictus* immediately after stabilization with 12% hexylene glycol, pH 6.3, at 22°C. Polarization microscopy, × 1,100. Scale division, 10 μm.

pH 6.3, washed twice with the isolation medium, postfixed for 30 min in 1% osmium tetroxide-12% hexylene glycol solution at pH 6.3, and washed twice for 5 min each with the isolation medium. Dehydration started with 30% ethanol-12% hexylene glycol solution, then 50% ethanol-12% hexylene glycol. Hexylene glycol was omitted from the graded concentrations of ethanol above 70%. Fixed isolated spindles can be stored in 100% ethanol overnight without altering their size and BR. After dehydration, spindles were placed in propylene oxide, followed with a mixture of equal proportions of propylene oxide and Epon (Epon 812, Shell Chemical Corp., San Francisco, Calif.). Embedding was accomplished in hard Epon (Luft, 1961) rather than Araldite to provide good preservation of fine structure without shrinkage or compression upon sectioning (Page and Huxley, 1963). Thin sections were cut with a diamond knife on a Porter-Blum Ultramicrotome MK-II (DuPont Instruments, Sorvall Operations, Newtown, Conn.), stained with uranyl acetate and lead citrate, and examined with a Philips model 200 electron microscope.

Although not commonly noted, rapid alteration of pH from 6.3 to 6.8 during spindle isolation produces dissociation and lateral splits of microtubules. Likewise, in the early steps of dehydration, change in pH or osmolarity can induce "C tubules" within isolated spindles even during or after glutaraldehyde or osmium tetroxide fixation (Sato, 1975).

Calculations

In Wiener's equation the form BR of rodlets is given as $(n_e^2 - n_o^2)$, the difference of dielectric constants or of the squares of the extraordinary and the ordinary refractive indices. This value is difficult to compare with specimen retardation which is the parameter measured. Fortunately, Bragg and Pippard (1953) have rederived the Wiener equation in a more general form which permits expression of form BR as $(n_e - n_o)$ which is the coefficient of BR (BR_{coeff}).

Bragg and Pippard give the equation for the dielectric constant experienced by an electric field in a particular direction relative to the orientation direction of a group of ellipsoids embedded in a medium of different refractive index as:

$$\epsilon = \epsilon_2 + \frac{f(\epsilon_1 - \epsilon_2)}{1 + (1 - f)\{(\epsilon_1 - \epsilon_2)/\epsilon_2\}L} \quad (2)$$

where ϵ is the average dielectric constant in the direction specified, ϵ_1 is the dielectric constant of the ellipsoids[1], ϵ_2 is the dielectric constant of the medium, f is the fraction of the total volume occupied by the ellipsoids, and L is the depolarizing coefficient for the given direction. Values of L, a geometric constant dependent on the ratios of the axes of the ellipsoids, have been tabulated by Stoner and cited in Bragg and Pippard. For ellipsoids of revolution whose polar axes are much greater than their equatorial axes (rodlets), L becomes zero for the field parallel to the polar axis and 0.5 for the field perpendicular to the polar axis. Since the index of refraction for nonabsorbing material is given by the square root of the dielectric constant experienced by its electric vector, the coefficient of BR for an assembly of rodlets is:

$$(n_e - n_o)_F = (\epsilon^{1/2} - \epsilon_\perp^{1/2})$$

$$= [\epsilon_2 + f(\epsilon_1 - \epsilon_2)]^{1/2} -$$

$$[\epsilon_2 + \frac{f(\epsilon_1 - \epsilon_2)}{1 + (1 - f)\{(\epsilon_1 - \epsilon_2)/\epsilon_2\}0.5}]^{1/2} \quad (3)$$

where ϵ is the dielectric constant (at light frequency) in the direction of the long axes of the rodlets (optic axis direction), and $\epsilon_\perp$ is the dielectric constant when the electric vector is perpendicular to the optic axis.

Since specimen BR was determined from the retardation it produced, we have chosen to analyze our data as BR retardation, $\Gamma = T(n_e - n_o)$, rather than as coefficient of BR, $(n_e - n_o)$. Additionally, the actual retardation may include some level of intrinsic BR. Accordingly we have included specimen thickness (T) and coefficient of intrinsic BR (I) as variables in the equation we use to plot our curves. Hence:

$$\Gamma = T\{I + (n_e - n_o)_F\}$$

$$= T\{I + [n_2^2 + f(n_1^2 - n_2^2)]^{1/2}$$

$$- [n_2^2 + \frac{f(n_1^2 - n_2^2)}{1 + (1 - f)\{(n_1^2 - n_2^2)/n_2^2\}0.5}]^{1/2} \quad (4)$$

where n_1 is the index of refraction of the rodlets, n_2 is the index of refraction of the medium and f is fraction of the volume occupied by the ellipsoids, which are now rodlets.

Calculations were performed on a programmable calculator (Hewlett Packard 9830A, Hewlett Packard Co., Loveland Division, Loveland, Colo.) with its associated printer and plotter. The calculator was programmed to calculate Γ according to the equation above for specified values of n_1, T, I, and f at each value of n_2 for which we had an observation. This calculated value was subtracted from each observed value and the result squared. The data points were then plotted on the chart together with the calculated curve. At the end of the curve the plotter printed the sum of the squared error.

Of the variables (n_1, f, I, and T), T can be determined at the time of retardation measurement to within about 1 μm, but the others are not directly measurable. Given a firm value for T and a set of data points, from a specific Wiener curve, the values of n_1, I, and f belonging to that curve may be uniquely determined by curve fitting. The calculator program facilitates this process by providing both a visual comparison of the curve with the data and a quantitative rating of the fit for each curve plotted.

The deviation of the calculated curve from the plotted data points reveals which variable is in need of adjustment. If the chosen n_1 is too great, the curve shifts toward a larger index relative to the data points; if n_1 is too small, the curve shifts toward lower index (Fig. 5). If the value used for f is too large, the extremes but not the trough of the curve are high relative to the data points and low if f is too small. Changes in I simply translate the curve *in toto* to higher or lower values with increase or decrease of I. An increase in T has the same effect as a simultaneous increase in I and f.

By this means, a good visual fit of the curve to the data points is quickly achieved. The values of n_1, f, and I obtained are good approximations of the final values and serve as excellent starting values to achieve rapid convergence in the optimization process to follow.

To improve the fit beyond that which could be achieved visually, we devised a program which employed the method of least squares (Frazer and Suzuki, 1973) to optimize the values of n_1, f, and I to fit the observed data and a given value of T. In this program the unweighted standard deviation (σ = square root of the mean squared error) was used to quantitate the fit of the curve to the data. The curve which best fit the data would be that for which σ was minimum. To find this curve, the values of

[1] Our use of subscript 1 for the ellipsoids and subscript 2 for the medium conforms with Wiener's original usage rather than that of Bragg and Pippard which is reversed.

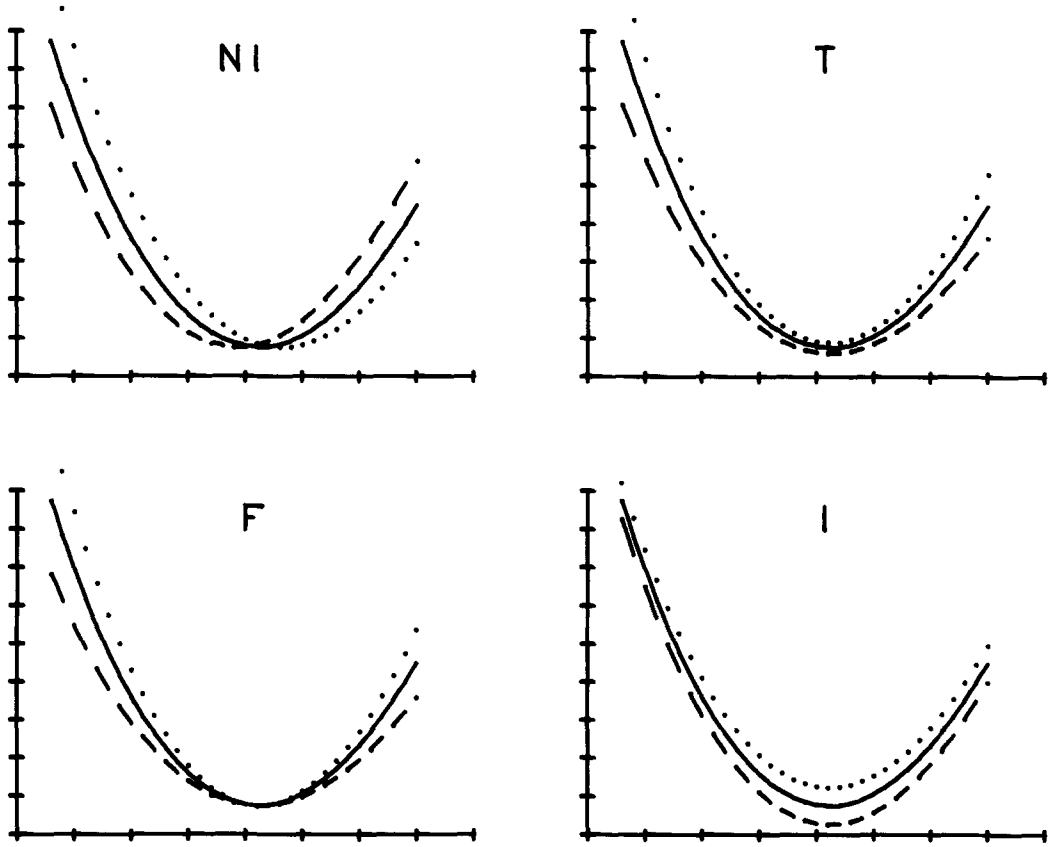

FIGURE 5 Plots of calculated Wiener curves showing effect of variation in the parameter with which each is labeled. For each parameter shown, the calculations have been made with the other parameters held constant at the values used for their solid curve. $N1$: solid curve, $n_1 = 1.512$; dotted curve, $n_1 = 1.532$; dashed curve, $n_1 = 1.492$. F: solid curve, $f = 0.0206$; dotted curve, $f = 0.0256$; dashed curve, $f = 0.0156$. T: solid curve, $T = 8.0\ \mu m$; dotted curve, $T = 9.5\ \mu m$; dashed curve, $T = 6.5\ \mu m$. I: solid curve, $I = 4.7 \times 10^{-6}$; dotted curve, $I = 7.7 \times 10^{-6}$; dashed curve, $I = 1.7 \times 10^{-6}$.

n_1, f, and I were varied systematically until σ was at a minimum with respect to alteration of the sixth significant digit of each of the variables. The resulting values of n_1, f, I, and σ were then accepted as optimum for fit for the curve to the data.

These values were then used in a second version of the first program, which plotted the data points and the best fit curve together with dotted curves marking the unweighted standard deviation (Figs. 6, 7, and 8).

FORM BR OF ISOLATED *PISASTER* SPINDLE

Results of Imbibition

Spindles isolated in 12% hexylene glycol and held at room temperature slowly lose their BR unless fixed (Kane and Forer, 1965). Consequently, during the period required for mounting the isolated spindles between gelatin pellicles in the Rose chamber before fixing, some spindle BR is lost. We estimate that the loss is no more than 10% on the basis of comparison with retardation measurements made on 340 fresh, unfixed isolates in 12% hexylene glycol in which we found a retardation of 3.82 nm ± 0.54 nm. This measurement was made on spindles unselected for size and cannot rigorously be compared with those used in the imbibition series since the latter were selected for similar spindle width (8 μm ± 0.5 μm). The mounted spindles had the same retardation, ~3.5 nm, in 12% hexylene glycol before and after fixation.

The imbibition media and their refractive in-

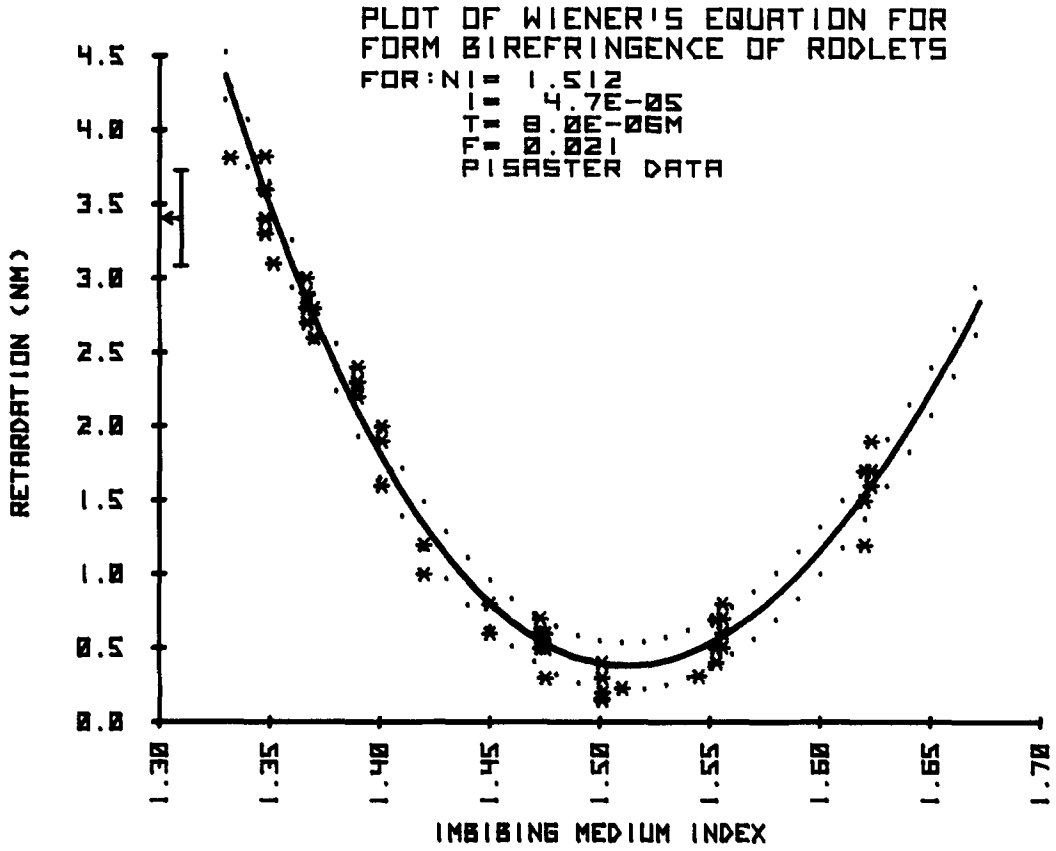

FIGURE 6 Machine plot of the best-fit Wiener curve (solid curve) with the *Pisaster* imbibition data points to which the curve was fitted. The total number of plotted points is 89, of which nearly half are coincident with others. The dotted curves represent the theoretical retardation at each point plus or minus the unweighted standard deviation of the theoretical curve as compared with the data as a whole. The error bar with arrow shown at the ordinate represents the mean and standard deviation of the retardation measured for 30 spindles in intact living *Pisaster* oocytes.

dices (n_2) are summarized in Table I. The points in Fig. 6 represent all the measurements on the 14 isolated spindles which showed total reversibility of retardation when returned to the initial medium of $n_2 = 1.348$. Each point represents the mean of triplicate measurements with an estimated error of not greater than 0.1 nm. The solid curve in Fig. 6 is the calculated Wiener curve optimized for a spindle thickness (T) of 8 μm. The dotted lines mark the unweighted standard deviation ($\pm$ 0.16 nm) for the fit of the calculated curve to the aggregate of all the data points. The agreement between the values measured for the isolated spindles and the calculated curve is excellent.

For the given spindle thickness the value obtained for f is 0.0206, for I is 4.7×10^{-5}, and the value for n_1 is 1.512. Since the values obtained for f and I are dependent on T, the optimization routine was performed for spindle thicknesses of 7.5 μm and 8.5 μm to determine the range of variation to be expected for f and I. At $T = 7.5$ μm, $f = 0.0219$ and I is 5.0×10^{-5}. At $T = 8.5$ μm, $f = 0.0193$ and I becomes 4.4×10^{-5}.

We have also indicated at the ordinate axis the range of retardations we have observed at 13°C in living *Pisaster* spindles. This is found to be 3.4 nm $\pm$ 0.32 nm. If compared with our calculated Wiener curve, this would suggest that the living spindle is in a medium (cytoplasm) having a refractive index of about 1.352 $\pm$ 0.008.

Effective Volume of Microtubule Subunit

For a variety of microtubule types, Tilney et al. (1973) have verified that each turn of the mi-

crotubule has 13 subunits or protofilaments. X-ray diffraction of wet microtubules (Cohen et al., 1971), in agreement with negative staining electron microscope measurements (Grimstone and Klug, 1966), shows both 4-nm and 8-nm longitudinal periods. The 8-nm repeats are stronger and may be considered to correspond to the length of the tubulin dimer. Both methods arrive at a protofilament width of about 5 nm. The surface lattice derived from X-ray diffraction (Cohen et al., 1971) was first thought to differ from that of Grimstone and Klug (1966), but recent findings have reconciled the difference in favor of the earlier lattice (Cohen et al., 1975). Erickson (1974), using optical reconstruction, reports a relatively complex shape for the subunits. Neither this method nor X-ray diffraction has yet yielded exact measurement of subunit volume.

Since we have determined the volume fraction of microtubules in the spindle, and since the microtubules approximate infinitely long rodlets, we can independently calculate the subunit volume, or the volume defended by the protofilament subunit as follows.

Electron micrographs of our isolated *Pisaster* spindles (Figs. 2 and 3) showed microtubules, almost exclusively, to be the predominant structural component. Measurements from cross sections (Fig. 2) taken from the same region that we used for retardation measurements (Fig. 1 A) showed the average density of microtubules across the 8 μm diameter to be 106 microtubules/μm^2.

Taking our values for f obtained from curve fitting and for the number of microtubules/μm^2 (M), we find as follows:

$$f = 0.0206$$

$$= \frac{\text{volume defended by rodlets}}{\text{unit volume of structure}}$$

$$= V_s \times S \times P \times M/\mu m^3$$

$$= V_s \times 125 \times 13 \times 106 \div 10^9\ nm^3/\mu m^3,$$

$$\text{and } V_s = 119.6\ nm^3\ (5),$$

where V_s is the protofilament subunit (dimer) volume, S is the number of subunits per μm of protofilament, and P is the number of protofilaments per microtubule.

If the dimeric subunits were right circular cylinders, their diameter would be about 4.4 nm. The presence of the 4-nm longitudinal repeat period in the X-ray data suggests that the dimers are not simple cylinders. If they were made up of two spheres merged at the center for a total length of 8 nm, the sphere diameter would be about 5.0 nm. We have not attempted to use the shape suggested by Erickson (1974) since it is undefined in the third dimension. Obviously an unlimited variety of shapes could be imagined which would equally fit the present constraints. However, if the shape deviates too much from being essentially cylindrical as a protofilament, this must be considered in the choice of the depolarizing coefficient L in Eq. 2.

Although the detailed shape and exact dimensions of the tubulin molecule *in situ* in the microtubule are yet to be determined, the preceding calculations show a good fit between the structural parameters obtained from X-ray diffraction, electron microscopy, and hydrodynamic considerations and the volume fraction value we obtained from the optimized Wiener curve.

FORM BR IN OTHER MATERIAL

Spindle in Bouin's-Fixed Cells

Fig. 7 shows imbibition data for a fixed spindle at anaphase onset in a 7-μm thick section of a sea urchin egg *Lytechinus* (*Toxopneustes*) *variegatus*. The slide with sections fixed in Bouin's solution and unstained was a gift of the late Dr. E. B. Harvey. Retardations were measured with a 29.4-nm Brace-Köhler compensator with the mercury green line, in Schillaber's oil (R. P. Cargille Labs Inc., Cedar Grove, N. J.), in the following sequence of imbibing medium refractive index: 1.51 → 1.80 → 1.70 → 1.60 → 1.50 → 1.40 → 1.45 → 1.55 → 1.65 → 1.75. The best fit Wiener rodlet BR curve was drawn by computer as described for the isolated spindle.

The BR of the fixed spindle at low imbibing medium index is severalfold higher (BR_{coeff} = $4.9 \cdot 10^{-3}$ for the form curve extrapolated to n_2 = 1.33) than the BR of *L. variegatus* spindles in living cells ($2\text{–}3 \cdot 10^{-4}$ depending on exact stage of division and on temperature) or of the isolated *P. ochraceus* spindle. We have noticed sharp rises in the BR of spindles in a variety of cells fixed with histological fixatives in which the spindles appear coarsely fibrillar (also see Satô, 1958).

The matching refractive index of the Bouin's-fixed *Lytechinus* spindle (1.552) is higher, and at match point the BR (BR_{coeff} = $3.0 \cdot 10^{-4}$) is larger, than the value for the isolated *Pisaster* spindle (Fig. 6). The volume fraction, f = 0.135, is

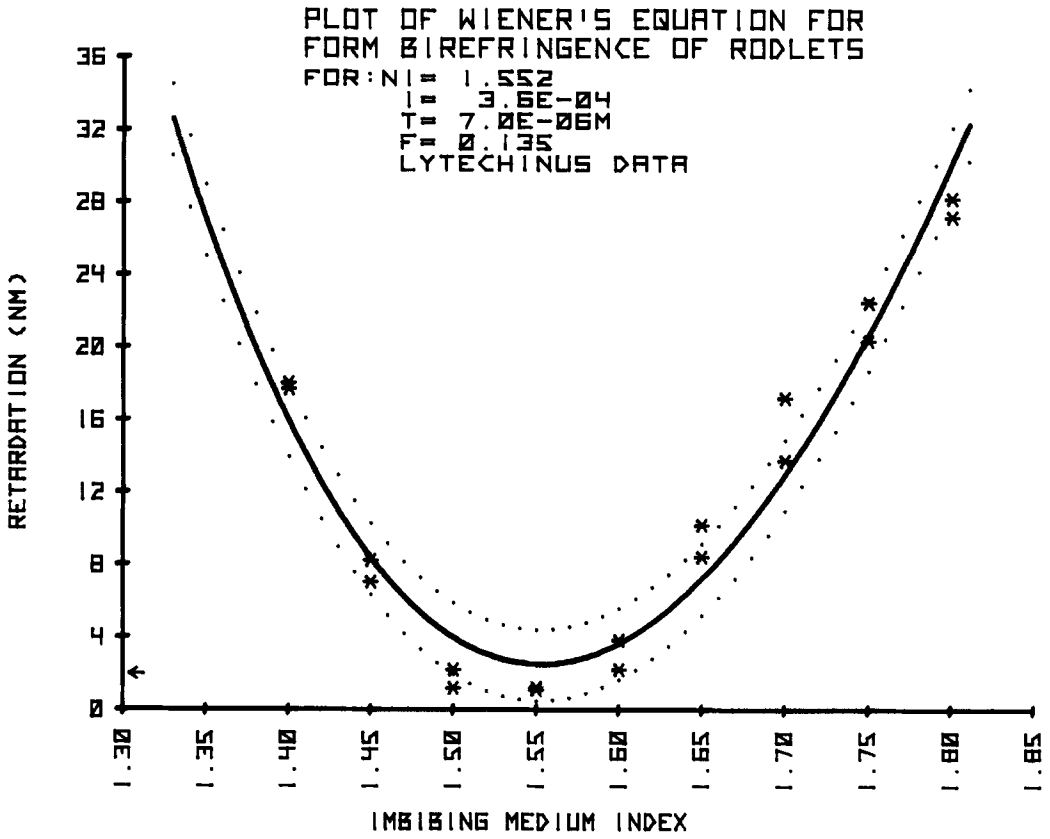

FIGURE 7 The data shown on this plot were obtained by imbibition of Bouin's-fixed spindle of *L. variegatus* zygote. It shows a large increase in rodlet volume fraction (f) and a slight increase in rodlet refractive index (n_1), both of which suggest that the fixative has produced a condensation of cytoplasmic materials onto the spindle microtubules. The arrow at the ordinate axis shows the average birefringent retardation measured for metaphase spindles in living *L. variegatus* zygotes.

severalfold larger than that obtained with isolated *Pisaster* spindles.

We interpret these observations to indicate the dense deposition of cytoplasmic components onto the microtubules which in turn may have formed coarse fibrillar aggregates.

Form BR of Skeletal Muscle

We have also examined the Wiener rodlet form BR in skeletal muscle. Fig. 8 shows imbibition data for the Q (= A) band obtained by Noll and Weber (1934) on frog cutaneous pectoris muscle fixed at 0–4°C with 5–10% formalin for 24 h (imbibition sequence shown in their Table IV), together with our computer derived best fit form BR curve. We obtain $n_1 = 1.526$, $I = 8.6 \times 10^{-4}$, and $f = 0.064$.

The form BR values given by our curve differ from those calculated by Noll and Weber who assumed the rodlet volume fraction to equal the fractional dry matter volume. The latter was calculated from the diameters of the muscle fiber measured in each imbibing medium compared to their diameter upon drying. The form BR calculated on this basis does not agree with their measured BR, varying with imbibing medium and showing discrepancies as high as fivefold (see Noll and Weber, 1934, their Table IV a).

Instead of total dry matter, we calculated the rodlet partial volume from cross-sectional dimensions of the overlapping A and I filaments seen in electron micrographs. The thick filaments measure 10–11 nm, and the thin filaments 5–6 nm in diameter (Huxley, 1960). X-ray diffraction studies of frog living sartorius muscle at rest length show the thick filaments to be hexagonally arranged with a center-to-center distance of 45 nm (Huxley,

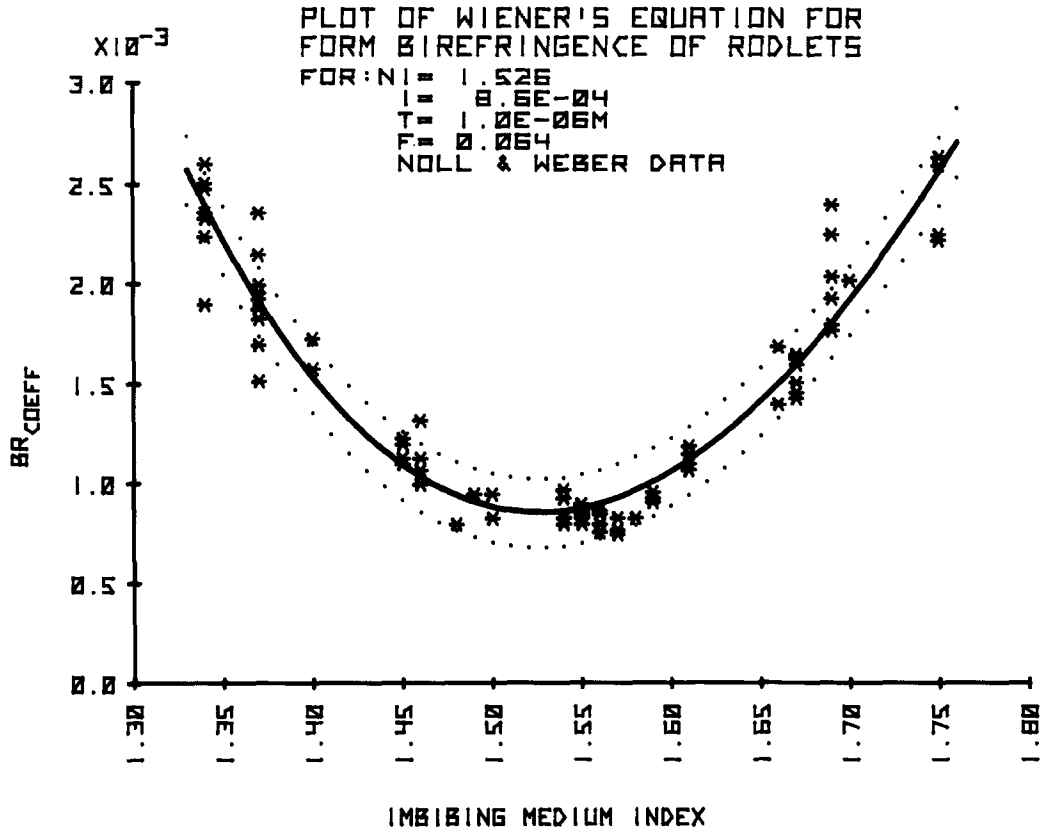

FIGURE 8 The data plotted are from Noll and Weber (1934) for the *A* band of frog sartorius muscle. In this case the ordinate represents coefficient of birefringence. The computer optimized Wiener curve shows a reasonably good fit to their data and yields a rodlet volume fraction (f = 0.064) close to the value we calculated from electron micrographs (see text).

1960). One thin filament is found at each trigonal point. The cross-sectional area which includes one thin and three one-sixths thick filaments is then 877 nm². The volume fraction of the thick and thin filaments together thus becomes 0.067–0.086. These values are in reasonable agreement with the partial volume 0.064 for the Wiener best fit curve shown in Fig. 8.

From myosin and actin contents of muscle, Cassim et al., (1968) calculate the *A*-band rodlet partial volume as 0.1–0.15. If, instead of total myosin and actin, one uses the lengths, particle weights, and partial specific volumes of the molecules making up the shaft portion only of the thick filament (12 1.6 nm diameter light meromyosin C rods per cross-section: Young et al., 1972) and the thin filament (two 70,000 dalton tropomyosin and 14 46,500 dalton actin monomers per 385 Å length: Pepe, 1972), one obtains a volume fraction of 0.041. Considering the variable contribution of myosin arms etc, one would expect the effective volume fraction to lie in between these values.

DISCUSSION

The validity of the Wiener formulation has been questioned on the basis of flow BR measurements of several "fibrous" proteins and rod-shaped viruses (Taylor and Cramer, 1963; Cassim and Taylor, 1965; Cassim et al., 1968). In its place, Cassim et al. propose the use of an empirical formula which equates BR_{coeff} to partial volume of the rodlets times specific BR in water where BR = $(1.7 \pm 1.3) \cdot 10^{-2}$. Using this formula, they calculate that for vertebrate skeletal muscle the total BR_{coeff} should be $(1.7\text{–}2.5) \cdot 10^{-3}$ and the intrinsic BR_{coeff} $(1\text{–}1.5) \cdot 10^{-3}$. Applied to the isolated *Pisaster* spindle, the BR_{coeff} should be $(1.4\text{–}2.0) \cdot 10^{-2} \cdot 0.021 = (2.9\text{–}4.2) \cdot 10^{-4}$ in water. While some of these values match the observed ones, the results of their formulation can depart as

much as severalfold (see Cassim et al. 1968, Fig. 6) from those obtained by using Wiener's equation which we have demonstrated to fit the measured BR over a wide range of imbibing medium refractive index.

In the application of the Ambronn imbibition method, alteration of the volume fraction f, or the index of refraction n_1, or of any factor necessitating the use of an alternate depolarizing factor L, for example, by interaction of the particles with the media, could lead to a departure from the Wiener relationship. This would be particularly important when the rodlets are not supported by an organized structure. Large changes in rodlet shape (for example by bending or coiling or conversely by stiffening) could have a drastic effect on the predictive value of the equation unless the changes are accounted for by selection of appropriate values of L.

The imbibition data of striated muscle A band obtained by Noll and Weber (1934) can be fitted to a Wiener curve yielding a reasonable volume fraction value. However, Noll and Weber found considerable lateral and some longitudinal shrinkage of the muscle exposed to the dehydrating and imbibition media. The index "match point" given for their dehydrated muscle is higher than the minimum of the best fit Wiener curve.

Further imbibition studies on myofibrils free from shrinkage and irreversible BR changes would seem to be in order since the observed reduction of the BR by overlap of the A- and I-filaments (Colby, 1971, and D. L. Taylor, personal communication) is likely to provide significant insight into the dynamics of actomyosin interaction in muscle contraction.

In the mitotic spindle, careful perfusion of the glutaraldehyde-fixed isolated spindles, sandwiched with pellicles of gelatin, introduced little microscopically visible dimensional change, and the BR was totally reversible when returned to the original low index medium. The fact that those preparations which maintained constant width gave reproducible BR values fitting the Wiener formula gives us confidence that Ambronn's imbibition method is indeed applicable to form BR analysis, and that the Wiener formulation is itself accurate. Furthermore, we note that there do exist many reports of imbibition results which display typical Wiener curves (see e.g. Ambronn and Frey, 1926; Chinn and Schmitt, 1937; Schmidt, 1951; and Bendet and Beardon, 1972).

The various parameters for Wiener rodlet form BR curves for the isolated, clean *Pisaster* meiotic spindles are summarized in Table II. The imbibed isolated spindles follow a theoretical Wiener curve for $f = 0.0206$. The retardation of the same spindle measured in intact oocytes at 13°C corresponds to the value of the Wiener curve at $n_2 = 1.352$.

On the basis of a disparity between the BR observed in living cells and the (very low) number and unexpected distribution of microtubules observed in their electron microscope sections, Behnke and Forer (1967) argued that microtubules are not responsible for spindle fiber BR in crane fly spermatocytes. Their argument has been disputed by Rebhun and Sander (1967) and Goldman and Rebhun (1969), and LaFountain (1974) has obtained electron micrographs of crane fly spermatocytes showing approximately 100 microtubules per μm^2 spindle cross section, clustered in regions corresponding to chromosomal fibers with higher BR. While concluding, as do Rebhun and his co-workers, that microtubules must be responsible for the major part of the form BR of the living spindle observed, LaFountain questions whether form BR of microtubules accounts for all of the spindle BR.

An exact accounting of all of the BR in a living spindle, as contrasted to a clean isolated spindle, demands that we at least know: (*a*) the refractive index of the intertubular material, (*b*) the distribution of angular divergence and lengths of the microtubules at each measured volume in the spindle, and (*c*) the fraction of microtubules and other components preserved for electron microscopy. Exact data are still missing on these points, and in fact the second and third points are known to be sensitive to many physiological and methodo-

TABLE II

Summary of Data from Isolated Pisaster Spindles

Rodlet refractive index	1.512
Rodlet volume fraction	0.0206
Average number of microtubules per μm^2	106
Average number microtubules per μm^2 for 6 μm diameter spindle core	130
Optically effective volume per tubulin dimer	120 nm^3
Coefficient of BR	5×10^{-4}
Intrinsic BR at match point (= 1.512)	4.7×10^{-5}
Estimated refractive index of cytoplasm	1.352

logical variables. Spindle BR in intact cells varies with temperature, pressure, osmotic pressure, pH, calcium ion concentration, tubulin availability, and exact stage of division. Parallel changes in microtubule behavior are found in vitro. Thus, these parameters would have to be carefully controlled at fixation and dehydration, and the change of BR, taking into account the refractive index of the imbibing media, would have to be closely monitored.

The data on Bouin's-fixed *Lytechinus* spindle presented above, and in Pfeiffer's (1951) report on the extraordinarily high form ($1 \cdot 10^{-3}$) and intrinsic ($4 \cdot 10^{-3}$) BR of spindles in a copepod egg and in the pollen tube of *Clivia* sp., clearly reflect examples of drastic alteration of spindle fine structure during fixation or dehydration, very probably by dense deposition of cytoplasmic components onto microtubules which in turn may have formed coarse aggregates. In fact Rebhun and Sander (1967), Goldman and Rebhun (1969) and Forer and Goldman (1972) have noted the presence of large amounts of ribosomes and other material paralleling the microtubules of isolated sea urchin spindles and have discussed their possible influence on BR. The intertubular materials adhere to the tubules to varying degrees depending on the pH and divalent cations present at the time of spindle isolation. Using interference microscopy, Forer and Goldman (1972) found the dry mass of washed isolated spindles to vary as a function of decreasing pH, from not more than 20% (pH 7.3) to 60% (pH 5.3) of their dry mass in intact eggs. Even in isolated spindles, Forer and Goldman (1972) have reported, especially at low pH, a rise of dry mass concentration when sea urchin spindles were preserved in a test tube. These effects need to be distinguished from genuine growth of microtubules in spindles and asters isolated in microtubule polymerizing solutions (Weisenberg, 1973; Weisenberg and Rosenfeld, 1975; Inoué et al., 1974; Rebhun et al., 1974).

Our estimate of the refractive index of the intertubular medium in living *Pisaster* oocytes (Table II) along with the data used to calculate microtubular subunit volume provides a means to calculate the fraction of the dry mass due to microtubules in intact cells. Where C is the concentration of dry mass in g/100 ml, and n is the refractive index (1.352), of the intertubular cytoplasm; n_s is the refractive index of the solvent (1.334); and α, the specific refractive increment is 0.0018, then: $n = n_s + \beta C$ (Barer and Joseph, 1954)

$$\text{or} \quad C = \frac{n - n_s}{\alpha} = \frac{1.352 - 1.334}{0.0018} = 10\ \text{g/100 ml.}$$

Using the notation of Eq. 5 and MW and N as subunit molecular weight and Avogadro's number, respectively, then the mass of microtubule per unit volume is:

$$S \times P \times M \times MW \div N$$
$$= 125 \times 13 \times 106 \times 110{,}000 \div 6.022 \times 10^{23}\ \text{g}/\mu\text{m}^3$$
$$= 3.15 \times 10^{-14}\ \text{g}/\mu\text{m}^3$$
$$= 3.15\ \text{g/100 ml}^2$$

If the total dry mass concentration in the intact living spindle is given by the sum of these, then microtubular dry mass contribution to the total is given by:

$$\frac{3.15}{10 + 3.15} = 0.24$$

Since some microtubules have probably been lost in spindle isolation (about 10%), this suggests that in the living *Pisaster* spindle the microtubular contribution to the dry mass is a minimum of 24%.

In the absence of extraneous material the microtubules yield an apparent refractive index of 1.512. This value is appreciably lower than the range of refractive index of dried protein cited in Taylor and Cramer (1963) (1.57–1.60). As Bragg and Pippard (1953) noted, the match point index does occur at a value considerably lower than that for dried protein, and they attributed the difference to a hydration shell. Barer and Joseph (1954) have called attention to a similar problem in cell refractometry and have cautioned that one cannot reliably go from the refractive index of a dried protein to its specific refractive increment in solution, or the reverse. Our finding reinforces these and points out the hazard inherent in attempting the prescriptive use of refractive index values from dried protein as starting points in Wiener calculations.

A number of authors have asked whether strain-induced BR may account for some of the spindle BR in living cells (Inoué and Dan, 1951; Allen,

[2] This is equivalent to a tubulin "concentration" of 31.5 mg/ml.

1972; LaFountain, 1972). Indeed, mechanically deformed gels do exhibit BR as do gels anisotropically swollen or dehydrated (Kunitz, 1930; Inoué, 1949). Whether similar strain BR does contribute to spindle BR can only be answered with further experimentation, but it would appear unlikely that the well oriented microtubules could appreciably contribute to strain BR. Strain BR would be expected by deformation of less well oriented gels such as those seen in isolated amoeba cytoplasm (Taylor et al., 1973), while increase in microtubular BR would be expected to reflect greater ordering and/or increase in microtubular concentration. We have found that change in orientation of even small clusters of (several to about ten parallel) microtubules can be detected with sensitive polarizing microscopes and, we believe, is distinguishable from changes in the quantity of regularly oriented microtubules.

This work was supported in parts by grant CA-10171 from the National Institutes of Health and grant GB-31739X from the National Science Foundation.

Received for publication 7 April 1975, and in revised form 1 July 1975.

REFERENCES

ALLEN, R. D. 1972. Pattern of birefringence in the giant amoeba, *Chaos carolinensis*. *Exp. Cell Res.* **72**:34–45.

AMBRONN, H., and A. FREY. 1926. Das Polarisationsmikroskop. Akademische Verlagsgesellschaft mbH. Leipzig, Germany.

BARER, R., and S. JOSEPH. 1954. Refractometry of living cells. I. Basic principles. *Q. J. Microsc. Sci.* **95**:399–423.

BEHNKE, O., and A. FORER. 1967. Some aspects of microtubules in spermatocyte meiosis in a crane fly (*Nephrotoma suturalis* Loew)—Intranuclear and intrachromosomal microtubules. *C. R. Trav. Lab. Carlsberg*. **35**:437–455.

BENDET, I. J., and J. BEARDEN, JR. 1972. Birefringence of spermatozoa. II. Form birefringence of bull sperm. *J. Cell Biol.* **55**:501–510.

BORN, M., and E. WOLF. 1959. Principles of Optics. Pergamon Press, Inc., New York.

BRAGG, W. L., and A. B. PIPPARD. 1953. The form birefringence of macromolecules. *Acta Crystallogr. Sect. B. Struct. Crystallogr. Chryst. Chem.* **6**:865–867.

BRYAN, J., and H. SATO. 1970. The isolation of the meiosis I spindle from the mature oocyte of *Pisaster ochraceous*. *Exp. Cell Res.* **59**:371–378.

CASSIM, J. Y., and E. W. TAYLOR. 1965. Intrinsic birefringence of poly-γ-benzyl-L-glutamate, a helical polypeptide, and the theory of birefringence. *Biophys. J.* **5**:531–551.

CASSIM, J. Y., P. S. TOBIAS, and E. W. TAYLOR. 1968. Birefringence of muscle proteins and the problem of structural birefringence. *Biochim. Biophys. Acta.* **168**:463–471.

CAVANAUGH, G. M. 1964. Formulae and Methods V. of the Marine Biological Laboratory Chemical Room. Marine Biological Laboratories, Woods Hole, Massachusetts.

CHINN, P., and F. O. SCHMITT. 1937. On the birefringence of nerve sheaths as studied in cross section. *J. Cell. Comp. Physiol.* **9**:289–296.

COHEN, C., D. DEROSIER, S. C. HARRISON, R. E. STEPHENS, and J. THOMAS. 1975. X-ray patterns from microtubules. *Ann. N. Y. Acad. Sci.* **253**: 53–59.

COHEN, C., S. C. HARRISON, and R. E. STEPHENS. 1971. X-ray diffraction from microtubules. *J. Mol. Biol.* **59**:375–380.

COLBY, R. H. 1971. Intrinsic birefringence of glycerinated myofibrils. *J. Cell Biol.* **51**:763–771.

ERICKSON, H. P. 1974. Microtubule surface lattice and subunit structure and observations on reassembly. *J. Cell Biol.* **60**:153–167.

FORER, A., and R. D. GOLDMAN. 1972. The concentrations of dry matter in mitotic apparatuses *in vivo* and after isolation from sea urchin zygotes. *J. Cell Sci.* **10**:387–418.

FRAZER, R. D. B., and E. SUZUKI. 1973. The use of least squares in data analysis. *In* Physical Principles and Techniques of Protein Chemistry. Part C. Syndney J. Leach, editor. Academic Press, Inc., New York.

GOLDMAN, R. D., and L. I. REBHUN. 1969. The structure and some properties of the isolated mitotic apparatus. *J. Cell Sci.* **4**:179–209.

GRIMSTONE, A. V., and A. KLUG. 1966. Observations on the substructure of flagellar fibres. *J. Cell Sci.* **1**:351–362.

HARTSHORNE, N. H., and A. STUART. 1960. Crystals and the Polarizing Microscope—A Handbook for Chemists and Others. 3rd. ed. Edward Arnold Publishers Ltd. London.

HUXLEY, H. E. 1960. Muscle cells. *In* The Cell. J. Brachet and A. E. Mirsky, editors. **4**:365–481. Academic Press, Inc., New York.

INOUÉ, S. 1949. Studies of the *Nereis* egg jelly with the polarization microscope. *Biol. Bull.* (*Woods Hole*). **97**:258–259.

INOUÉ, S., G. G. BORISY, and D. P. KIEHART. 1974. Growth and lability of *Chaetopterus* oocyte mitotic spindles isolated in the presence of porcine brain tubulin. *J. Cell Biol.* **62**:175–184.

INOUÉ, S., and K. DAN. 1951. Birefringence of the dividing cell. *J. Morphol.* **89**:423–455.

INOUÉ, S., J. FUSELER, E. SALMON, and G. W. ELLIS. 1975. Functional organization of mitotic microtubules: physical chemistry of the *in vivo* equilibrium system. *Biophys. J.* **15**:725–744.

INOUÉ, S., and W. L. HYDE. 1957. Studies on depolarization of light at microscope lens surfaces. II. The simultaneous realization of high resolution and high

sensitivity with the polarizing microscope. *J. Biophys. Biochem. Cytol.* **3**:831–838.

INOUÉ, S., and H. RITTER, JR. 1975. Dynamics of mitotic spindle organization and function. *In* Molecules and Cell Movement. R. E. Stephens and S. Inoué, editors. Raven Press, New York. 3–31.

INOUÉ, S., and H. SATO. 1967. Cell motility by labile association of molecules. The nature of mitotic spindle fibers and their role in chromosome movement. *J. Gen. Physiol.* **50**:259–292.

KANATANI, H., H. SHIRAI, K. NAKANISHI, and T. KUROKAWA. 1969. Isolation and identification of meiosis inducing substance in starfish *Asterias amurensis*. *Nature (Lond.)*. **221**:273–274.

KANE, R. E. 1962. The mitotic apparatus: isolation by controlled pH. *J. Cell Biol.* **12**:47–55.

KANE, R. E. 1965. The mitotic apparatus: physical-chemical factors controlling stability. *J. Cell Biol.* **25**:137–144.

KANE, R. E., and A. FORER. 1965. The mitotic apparatus. Structural changes after isolation. *J. Cell Biol.* **25**:31–39.

KUNITZ, M. 1930. Elasticity, double refraction and swelling of isoelectric gelatin. *J. Gen. Physiol.* **13**:565–606.

LAFOUNTAIN, J. R. 1972. Changes in the patterns of birefringence and filament deployment in the meiotic spindle of *Nephrotoma suturalis* during the first meiotic division. *Protoplasma.* **75**:1–17.

LAFOUNTAIN, J. R. 1974. Birefringence and fine structure of spindles in spermatocytes of *Nephrotoma suturalis* at metaphase of first meiotic division. *J. Ultrastruct. Res.* **46**:268–278.

LUFT, J. H. 1961. Improvement in epoxy resin embedding methods. *J. Cell Biol.*, **9**:409–414.

MOLÈ-BAJER, J., and A. BAJER. 1968. Studies of selected endosperm cells with the light and electron microscope. The technique. *LaCellule.* **67**:257–265.

NOLL, D., and H. H. WEBER. 1934. Polarisationsoptik und molekularer Feinbau der Q-Abschnitte des Froschmuskels. *Pflügers Arch.* **235**:234–246.

OLMSTED, J. B., and G. G. BORISY. 1973. Microtubules. *Ann. Rev. Biochem.* **42**:507–540.

PAGE, S. G., and H. E. HUXLEY. 1963. Filament lengths in striated muscle. *J. Cell Biol.* **19**:369–390.

PEPE, F. A. 1972. The myosin filament: immunochemical and ultrastructural approaches to molecular organization. *Cold Spring Harbor Symp. Quant. Biol.* **37**:97–108.

PFEIFFER, H. H. 1951. Polarisationsoptische Untersuchungen am Spindelapparat mitotischer Zellen. *Cytologia (Tokyo)* **16**:194–200.

REBHUN, L. I., J. ROSENBAUM, P. LEFEBVRE, and G. SMITH. 1974. Reversible restoration of the birefringence of cold-treated isolated mitotic apparatuses of surf clam eggs with chick brain tubulin. *Nature (Lond.)*. **249**:113–115.

REBHUN, L. I., and G. SANDER. 1967. Ultrastructure and birefringence of the isolated mitotic apparatus of marine eggs. *J. Cell Biol.* **34**:859–883.

SATO, H. 1975. The mitotic spindle. *In* Aging Gametes. R. Blandau, editor. S. Karger AG, Basel. 19–49.

SATO, H., and J. Bryan. 1968. Kinetic analysis of association-dissociation reaction in the mitotic spindle. *J. Cell Biol.* **39**(2, Pt. 2):118 *a* (Abstr.).

SATÔ, S. 1958. Electron microscope studies on the mitotic figure. I. Fine structure of the metaphase spindle. *Cytologia (Tokyo)* **23**:383–394.

SCHMIDT, W. J. 1951. Polarisationsoptische Analyse der Verknupfung von Protein und Lipoidmolekeln, erlautert am Aussenglied der Sehzellen der Wirbeltiere. *Publ. Stn. Zool. Napoli.* **23**(Suppl.):158–183.

STEPHENS, R. E. 1972. Studies on the development of the sea urchin *Strongylocentrotus droebachiensis*. II. Regulation of mitotic spindle equilibrium by environmental temperature. *Biol. Bull. (Woods Hole)* **142**:145–159.

TAYLOR, D. L., J. S. CONDEELIS, P. L. MOORE, and R. D. ALLEN. 1973. The contractile basis of amoeboid movement. I. The chemical control of motility in isolated cytoplasm. *J. Cell Biol.* **59**:378–394.

TAYLOR, E. W., and W. CRAMER. 1963. Birefringence of protein solutions and biological systems. I. *Biophys. J.* **3**:127–141.

TILNEY, L. G., J. BRYAN, D. J. BUSH, K. FUJIWARA, M. S. MOOSEKER, D. B. MURPHY, and D. H. SNYDER. 1973. Microtubules: evidence for 13 protofilaments. *J. Cell Biol.* **59**:267–275.

WEISENBERG, R. C. 1972. Microtubule formation *in vitro* in solutions containing low calcium concentrations. *Science (Wash. D. C.)*. **177**:1104–1105.

WEISENBERG, R. C. 1973. Regulation of tubulin organization during meiosis. *Am. Zool.* **13**:981–987.

WEISENBERG, R. C., and A. C. ROSENFELD. 1975. In vitro polymerization of microtubules into asters and spindles in homogenates of surf clam eggs. *J. Cell Biol.* **64**:146–158.

WIENER, O. 1912. Die Theorie des Mischkörpers für das Feld der stationären Strömung. *Abh. Sächs. Ges. Akad. Wiss., Math.-Phys. Kl.* No. 6, **32**:509–604.

YOUNG, M., M. V. KING, D. S. O'HARA, and P. J. MOLBERG. 1972. Studies on the structure and assembly pattern of the light meromyosin section of the myosin rod. *Cold Spring Harbor Symp. Quant. Biol.* **37**:65–76.